Geobiology

Geobiology (2011), 9, 250–265 DOI: 10.1111/j.1472-4669.2011.00273.x

Inverse carbon isotope patterns of lipids and kerogen record heterogeneous primary biomass

H. G. CLOSE, R. BOVEE AND A. PEARSON

Department of Earth & Planetary Sciences, Harvard University, Cambridge, MA, USA

ABSTRACT

Throughout the Proterozoic $\delta^{13}C$ values for preserved *n*-alkyl lipids are more positive than for syngenetic kerogen. This pattern is the inverse of biosynthetic expectations. It has been suggested that this isotopic inversion results from selective preservation of lipids from ^{13}C-enriched heterotrophic populations, while the bulk of kerogen derives from primary producers. Here, we formulate a degradation model to calculate the ^{13}C content of sedimentary total organic carbon and lipid. The model addresses two scenarios. The first scenario explores preferential preservation of heterotrophic lipid, thereby quantifying the existing hypothesis. In the second, we suggest that an inverse signature could be the result of prokaryotic phytoplankton contributing the majority of the total ecosystem biomass. Photosynthetic prokaryotes bearing a relative ^{13}C enrichment would contribute much of the resulting preserved lipids, while primary eukaryotic biomass would dominate the total organic carbon. We find that our hypothesis of a mixed primary producer community generates inverse isotopic patterns while placing far fewer requirements on specific degradation conditions. It also provides a possible explanation as to why there are large variations in the ^{13}C content of the isoprenoid lipids pristane and phytane relative to *n*-alkyl lipid, while the difference between *n*-alkyl lipid and kerogen is more constant. Our results suggest that the disappearance of the inverse ^{13}C signature in the late Ediacaran is a natural consequence of the fundamental shift to oceans in which export production has a higher ratio of eukaryotic biomass.

Received 18 August 2010; accepted 25 January 2011

Corresponding author: Hilary G. Close. Tel.: 617-496-3299; fax: 617-495-8839; e-mail: hclose@fas.harvard.edu

INTRODUCTION

Organic matter in Precambrian marine deposits consistently has a carbon isotope relationship between *n*-alkyl lipids and total organic carbon (TOC) that is the reverse of what is observed throughout most of the Phanerozoic (Logan *et al.*, 1995; Brocks *et al.*, 2003b). Nearly all sedimentary rocks from the Phanerozoic have the isotopic ordering expected from direct biosynthetic products of Calvin–Benson–Bassham (Rubisco-utilizing) photoautotrophs (Fig. 1A), with average kerogen or TOC enriched in ^{13}C relative to bitumen; and within bitumen, isoprenoid lipids are ^{13}C-enriched relative to *n*-alkyl lipids (Hayes *et al.*, 1983; Hayes, 2001; Logan *et al.*, 1997). These compound classes in Proterozoic marine deposits consistently show the opposite ordering (Fig. 1B). Bitumen or extractable *n*-alkyl lipids (specifically, *n*-alkanes) are the most ^{13}C-enriched fraction; and although isoprenoids such as pristane and phytane can be ^{13}C-enriched or depleted relative to kerogen, consistently they are ^{13}C-depleted relative to *n*-alkyl lipids. The inverse patterns disappear in the late Ediacaran (Logan *et al.*, 1995, 1997; Höld *et al.*, 1999; Kelly, 2009), but temporarily return in the late Permian where there is geochemical evidence for widespread ocean anoxia and photic zone euxinia (Grice *et al.*, 1996, 2005; Schwab & Spangenberg, 2004; Hays, 2010; Nabbefeld *et al.*, 2010). Inverse ordering of *n*-alkyl lipids vs. isoprenoids is present in these Permian deposits and also occurs rarely in other Phanerozoic deposits (Upper Ordovician: Guthrie, 1996; Upper Devonian: Joachimski *et al.*, 2001; Lower Jurassic: Schwab & Spangenberg, 2007; Upper Jurassic: van Kaam-Peters *et al.*, 1997; Dawson *et al.*, 2007; Upper Cretaceous: Hayes *et al.*, 1990; Eocene–Oligocene: Hollander *et al.*, 1993). However, most of these instances from the Phanerozoic are not accompanied by data indicating inverse ordering of *n*-alkyl lipids vs. TOC.

Although the Precambrian isotope pattern is termed 'inverse' because it is the opposite of our biosynthetic understanding, most of Earth history records this pattern. Marine deposits from the middle Proterozoic (~1055 Ma) through the late Neoproterozoic exclusively show inverse ordering. Additional observations suggest that the same signature was also prevalent in the Archean (Brocks *et al.*, 2003a,b). The

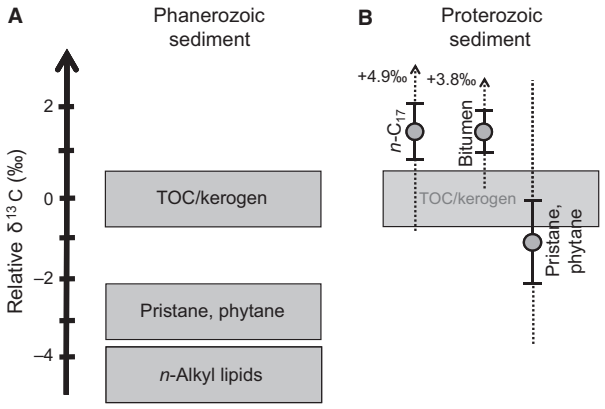

Fig. 1 (A) Relative values of $\delta^{13}C$ for organic components in typical Phanerozoic sediments, in agreement with expected biochemical patterns of fractionation (Logan *et al.*, 1995; Hayes, 2001). (B) Relative values of $\delta^{13}C$ for lipids relative to TOC or kerogen in Proterozoic sediments, averaged from Hieshima (1992) and Logan *et al.* (1995, 1997). Values show average and standard deviation (1σ), and the total range of individual values is shown with dotted lines.

Proterozoic data span marine deposits on several modern-day continents and thus potentially can be thought to constitute a global oceanic signature, although Precambrian deposits in general are limited to shelf–slope or epicontinental marine facies.

Before the advent of compound-specific isotope analysis, comparison of Proterozoic bitumens and kerogens exposed the inverse pattern, but it was thought to reflect contamination (Hoering, 1965, 1967). Further measurements showed that the inverse signature was syngenetic (Hieshima, 1992); and subsequently, compound-specific data revealed the ^{13}C-enriched *n*-alkyl pool within the bitumens (Logan *et al.*, 1995). These early reports of an inverse isotope signature for the Proterozoic focused on the consistency of positive values of $\Delta\delta = \Delta\delta_{n\text{-alkyl}} - \delta_{\text{kerogen/TOC}}$, which average ~1.5‰ (Fig. 1B) (Hieshima, 1992; Logan *et al.*, 1995; for discussion of terminological use of kerogen vs. TOC, see Supporting Information). Isotopic ordering of *n*-C_{17} alkane vs. kerogen, pristane vs. kerogen, and the average of *n*-C_{17} and *n*-C_{18} alkanes vs. pristane all upheld the inverse relationship. Subsequent reports have used these diagnostic compounds, as well as phytane, as the standard methods to monitor inverse isotope signatures (Logan *et al.*, 1997; Kelly, 2009).

Despite the geologic importance of these patterns, a satisfactory explanation remains elusive. Logan *et al.* (1995) suggested that a specific relationship between organic matter source and degradation existed in the Precambrian. Pristane and kerogen were proposed to derive mostly from photosynthetic species, thereby carrying the isotopic signature of carbon fixation. While kerogen may form from organic matter that survives remineralization due to biochemical resistance to degradation, association with ballast or mineral surfaces, or geopolymerization or reduction reactions (e.g. Hebting *et al.*, 2006; recent review by Zonneveld *et al.*, 2010), the Logan *et al.* (1995) hypothesis specifically invokes resistant algal biopolymer. After intense microbial heterotrophy in a water column largely devoid of eukaryotic grazers, *n*-alkyl lipids from primary producers were proposed to be replaced by *n*-alkyl lipids from heterotrophs. Heterotrophs would have been enriched in ^{13}C by the fractionation associated with intense respiration through multiple trophic levels (DeNiro & Epstein, 1978). Consequently, preserved TOC would consist of a mixture of primary kerogen and secondary lipid. With the diversification of multicellular Eukaryotes across the Cambrian boundary, an increase in the flux of faster-sinking particles (fecal pellets or increased biomineralization) concomitantly would increase the preservation potential of total primary material (including primary lipids) while reducing the intensity of water-column heterotrophy. This would decrease the degree of ^{13}C-enrichment in lipids from microbial heterotrophs, as well as the quantity of these lipids, eliminating the inverse isotope pattern.

The central premise of Logan *et al.* (1995) is that intense heterotrophy occurred in a water column dominated by small, slowly sinking cells. However, a persistent question remains as to how lipids from heterotrophs could dominate the total preserved lipids, especially considering that their biomass production rate can only constitute a fraction of total photosynthesis (e.g. del Giorgio & Cole, 1998), and both primary and secondary cells would be subjected to degradation in the same water column. Here, we quantitatively model the contributions of primary and heterotrophic organisms to TOC and lipids to answer this question. Our results suggest that the most physically plausible scenarios that generate inverse ^{13}C signatures are consistent with the origin of the ^{13}C enrichment within primary biomass. The disappearance of the inverse ^{13}C signature in the late Ediacaran would then represent a fundamental shift in the marine primary producer community, while episodic returns to inverse ordering in the Phanerozoic would signal a temporary return to higher prokaryote:eukaryote ratios, similar to Proterozoic oceans.

HETEROTROPHIC ENRICHMENT SCENARIO

To yield a carbon isotopic relationship in which preserved *n*-alkyl lipids are ^{13}C-enriched relative to TOC (positive value of $\Delta\delta_{n\text{-alkyl–TOC}}$), the lipid must carry an *integrated* isotopic value that is enriched in ^{13}C sufficiently to overcome what usually is a ~4.5‰ ^{13}C-depletion for lipid biosynthetic products relative to biomass (e.g. Teece *et al.*, 1999; Hayes, 2001). Accordingly, a model that considers the degradation rates (*K*) of all biomolecular classes to be equal cannot yield sufficient ^{13}C partitioning into net preserved lipids to produce a positive value of $\Delta\delta_{n\text{-alkyl–TOC}}$ (Supporting Information, Case 1). Therefore, the Logan *et al.* (1995) explanation implicitly requires different degradation potentials for different classes of biological products. Namely, recalcitrant carbon deriving from primary photosynthetic sources must comprise

the majority of kerogen. Lipids also must be resistant to degradation, because they are presumed to accumulate during late-stage processing. They must outlast the more labile components of biomass during diagenesis.

Following the models of several authors, we assume that both total organic matter and individual compound classes degrade following pseudo-first-order kinetics (Westrich & Berner, 1984; Middelburg, 1989). As the sedimentary record preserves organic matter after some total extent of degradation, we use d (degradation) rather than t (time) to represent the net decay in a particular environment. The parameter d is similar conceptually to the idea of total exposure (Hartnett *et al.*, 1998; Hedges *et al.*, 1999), and thus it is not strictly temporal but also can encompass environmental or biological factors relating to degradation intensity (e.g. Middelburg *et al.*, 1993; Rothman & Forney, 2007). It is well established that organic molecular classes degrade at different rates, typically $K_{\text{biopolymer}} < K_{\text{lipid}} < K_{\text{carbohydrate}} \sim K_{\text{protein}} << K_{\text{nucleic acid}}$ (Henrichs, 1992; Harvey *et al.*, 1995; Harvey & Macko, 1997; Grossi *et al.*, 2001; Versteegh & Zonneveld, 2002; Nguyen *et al.*, 2003). For the model, we consider the resistant (R) fraction to be equivalent in relative reactivity to biopolymer, but not necessarily composed exclusively or specifically of chemically resistant biomolecules such as algaenan, which may be less common than previously thought (Kodner *et al.*, 2009). We aggregate carbohydrate, protein, and nucleic acid as 'labile biomass' (B); and we treat lipid separately (L). The rate constants K_R, K_L and K_B are modeled accordingly such that $K_R < K_L < K_B$ (Table 1), with a minimum K_L/K_R constrained by the requirement of retaining at least 1 ppm lipid preserved within the sedimentary organic pool (details in Supporting Information).

Table 1 Model parameters and values

Model parameters	Symbol	Value used in examples	Range for Monte Carlo simulations
Biosynthetic fractionation, resistant biopolymer	ε_R	1.5‰	−1.5‰ to 4.5‰
Biosynthetic fractionation, *n*-alkyl lipid	ε_L	4.5‰	3–6‰
Degradation rate constant, resistant biopolymer	K_R	0.1	Fixed
Degradation rate constant, lipid	K_L	0.27	0.1–0.27
Degradation rate constant, labile biomass	K_B	10	Fixed
Fraction resistant biopolymer, primary producer cell	F_R	30%	15–35% ($1 - F_B - F_L$)
Fraction lipid, primary producer cell	F_L	10%	5–25%
Fraction labile biomass, primary producer cell	F_B	60%	Fixed
Fraction lipid, heterotrophic cell	F_{HL}	10%	5–25%
Fraction labile biomass, heterotrophic cell	F_{HB}	90%	75–95% ($1 - F_{HL}$)
Maximum heterotrophic ^{13}C enrichment per trophic level	h	1.5‰	1–2‰
Heterotrophic efficiency	E	0.3	0.05–0.6

The model also requires the assessment of carbon isotopic enrichment within the microbial food web. Critically, microbes do not feed by phagocytosis. They subsist on substrates generally <1000 Da, and a given organism may consume carbon deriving from lysis of multiple cells of different trophic histories (e.g. Jahnke & Craven, 1995). We introduce the concept here of 'molecular trophic level' rather than 'species trophic level' to clarify that higher trophic-level carbon is simply the net material which has been processed (incorporated or exuded) before respiration to CO_2. Thus, the net trophic hierarchy of a mixed microbial community is also a function of d. Consequently, trophic levels are not necessarily separated in time or space, and the net trophic level N is a parameter of the community, not of a single cell.

With these considerations, we incorporate differential degradation rates K_R, K_L and K_B to calculate the total preserved organic carbon (P) as a function of d

$$P(d) = \sum P_N(d) \tag{1}$$

and the isotopic composition of this organic carbon (P) and of lipid (L)

$$\delta_P(d) = \sum \frac{P_N(d)\delta_{P_N}(d)}{P(d)} \tag{2}$$

$$\delta_L(d) = \sum \frac{L_N(d)\delta_{\bar{L}}(d)}{L(d)} \tag{3}$$

for two scenarios: uniform exposure d, and attenuated exposure $D(d, N)$, in which there is less degradation at higher levels of N. Full details of all derivations and equations are given in the Supporting Information.

Uniform degradation of all trophic levels

To calculate the amount and isotopic signature of preserved organic matter, it is partitioned into material that remains unaltered from the original primary pool (P_0) and material that builds up from each subsequent addition of heterotrophic biomass (P_N). Photosynthetic biomass is modeled in three components: 'R', 'L' and 'B'. Heterotrophic cells are modeled as containing only 'L' and 'B', as bacteria are not known to produce chemically resistant biopolymers comparable to those observed in eukaryotic algae (Allard *et al.*, 1997). E is the overall heterotrophic efficiency (fraction of carbon incorporated into biomass; $1 - E$ = fraction respired as CO_2).

The isotopic signature of organic matter preserved in higher trophic levels ($N > 0$) depends on the isotopic value inherited from the degraded portion of the previous trophic level, and it subsequently is enriched by a weighted standard effect of heterotrophy, $h(1 - E)$ (h = 1.5‰; DeNiro & Epstein, 1978). Summing weighted isotopic contributions over all trophic levels, according to equations (2) and (3) above, yields the 'sedimentary' isotopic values for TOC and lipids, where lipid in each trophic level (δ_{L_N}) is correspondingly offset by the biosynthetic fractionation, ε_L = 4.5‰.

Attenuated degradation

A modified model captures the possibility of shorter exposure times for later molecular trophic levels, N. This simulates potential decreases in the degradation probability due to differences in physical location or environmental conditions; e.g. biosynthesis in sediments rather than in the water column, exposure of higher trophic levels to lower-oxygen environments, variations in rate of lysis, or decreases in reactivity due to geopolymerization and/or reduction via sulfur species (e.g. Hebting *et al.*, 2006). We model this effective exposure (D) for a given trophic level as an exponentially decreasing fraction of the maximum exposure: $D(d,N) = de^{-\zeta N}$, where the maximum (d) is experienced only by primary organic matter. Examples of scaling coefficients (ζ) and their influence on effective exposure time are shown in the Supporting Information, Fig. S2.

Parameter values

Both the constant-degradation and attenuated-degradation models were evaluated with regard to their ability to generate a positive value of $\Delta\delta_{n\text{-alkyl–TOC}}$. The maximum possible $\Delta\delta$ for a given parameterization was calculated using the following three constraints on the terminal level of d: (i) total preserved organic matter is not <0.01% of the original amount of photosynthetic product, comparable to intensive degradation regimes in the modern ocean (Martin *et al.*, 1987; Hedges & Keil, 1995; Wakeham *et al.*, 1997), and (ii) total preserved lipid is at least 1 ppm of the total sedimentary organic matter, such that enough would remain for lipid extraction and identification (includes both kerogen-bound and extractable lipid; see Supporting Information). We define these conditions as terminal burial. Finally, (iii) the total number of trophic levels through which the organic matter is processed increases until the available organic substrate from the preceding trophic level has decreased to 0.00001% of the original photosynthetic product, a value found to consistently approximate food chains that run to infinity. We define this as terminal heterotrophy, and it was found to reach a maximum of 14 trophic levels at $E = 0.3$, with the actual number depending on degree of exposure (d) and value of ζ. Model runs were terminated when one of the three boundary limits was reached. The models were initiated with the values shown in Table 1.

Results of heterotrophic enrichment scenarios

Constant d

A scenario of intense microbial reworking in the surface ocean would be expected to result in uniform (and high) degradation of organic matter through all trophic levels. Our model shows that such intense processing restricts the ability to create a positive value of $\Delta\delta_{n\text{-alkyl–TOC}}$ (Fig. 2). The net value of $\Delta\delta$ never exceeds zero, as the compounded decrease in biomass at each subsequent trophic level dictates progressively smaller contributions as N increases. Additionally, because some amount of lipid from P_0 always remains, the theoretical maximum value of $\Delta\delta$ that would arise from purely heterotrophic contribution to lipid cannot be reached at any extent of d. Heterotrophic enrichment therefore is maximized at intermediate d (Fig. 2A), but $\Delta\delta_{n\text{-alkyl–TOC}}$ is still negative. Thus, formation of a positive signature for $\Delta\delta_{n\text{-alkyl–TOC}}$ under this scenario is strictly dependent on the exact fractionations involved in biosynthesis, namely the values of ε_R, ε_L and h, where $\Delta\delta_{n\text{-alkyl–TOC}} \approx \varepsilon_R - \varepsilon_L + h(1 - E)$. In particular, to achieve a positive value of $\Delta\delta$ would require that the biopolymer or other material destined to become kerogen is systematically more isotopically negative, or lipids more isotopically

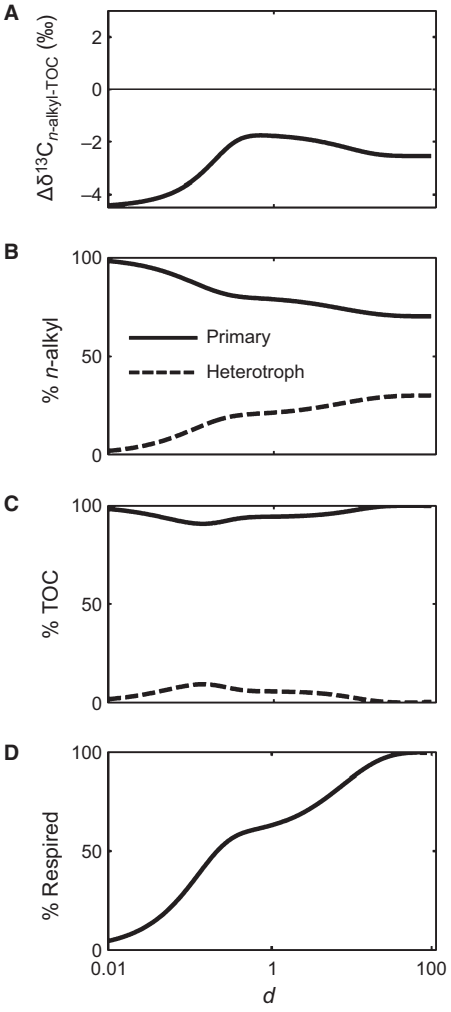

Fig. 2 Results of Logan-type scenario with d constant for all trophic levels. (A) Dependence of $\Delta\delta_{n\text{-alkyl–TOC}}$ on overall degradation, d. (B,C) Contributions of primary and heterotrophic populations to final preserved lipid and TOC. (D) Net respiration of primary productivity as a function of d.

positive, than could be reasonably expected based on known biosynthetic fractionations (Table 1).

Attenuated d

When $D(d,N) = de^{-\zeta N}$, later trophic levels experience less degradation. This leads to preferential preservation of biomass from later-stage heterotrophs, i.e. formalization of the scenario presented in Logan *et al.* (1995). Extreme attenuation (high ζ) favors preservation of heterotrophic material in excess of primary material, whereas extreme exposure (low ζ) favors preservation of only the most highly resistant primary material. Importantly, such attenuation of exposure time with trophic level does produce a positive value of $\Delta\delta_{n\text{-alkyl–TOC}}$, as postulated by Logan *et al.* (1995). Figure 3(A) shows that this outcome happens only in systems with moderately attenuated exposure times and over a narrow range of *d*. Under extreme attenuation, the amount of degradation experienced at higher trophic levels (high *N*) relative to level 0 is very small, especially at a high value of *d*. The result is that primary organic matter (P_0) approaches zero concentration, and all preserved lipid *and* total organic matter both derive from heterotrophs (top right corner of Fig. 3B,C). The final Δδ value approaches zero as the TOC becomes dominated by heterotrophic lipids (top right corner of Fig. 3A). Conversely, in the limit of a very small attenuation exponent (i.e. extreme exposure; bottom of Fig. 3A), the Δδ result follows the same pattern as Fig. 2A, and a positive isotope anomaly is never reached.

Intermediate values of ζ therefore are required to preserve heterotrophic lipids simultaneously with residual primary material. The area of positive $\Delta\delta_{n\text{-alkyl–TOC}}$ values in Fig. 3A maps well to the intersecting areas of high contribution of heterotrophic lipid to total preserved lipid (Fig. 3B), while still leaving the majority of total preserved organic matter as resistant biopolymer from P_0 (Fig. 3C). Values for Δδ become slightly to strongly positive (maximum of ~4.3‰) before the model run terminates. The maximum occurs at $\zeta \sim 0.15$. The magnitude of the maximum Δδ value is strongly dependent on when the model run is terminated, i.e. on how we choose the imposed limits of terminal heterotrophy and/or terminal burial. Note that the units of the *d* axes in Figs 2 and 3 are in the units of relative degradation and should not be equated to time. Rather, the distance along this axis represents the fractional approach to one of the criteria (i)–(iii), above. Accordingly, net respiration of primary productivity as a function of *d* is nearly identical for different values of ζ (Fig. 3D).

The dual variable space of *d* and ζ potentially can simulate environmental characteristics of the water column. For example, rapid attenuation and low total extent of degradation might occur in shallow water columns (rapid burial). Modest attenuation and degradation might occur in anoxic waters, and no attenuation and high extent of total degradation might reflect well-oxygenated open oceans. The concept of ζ encompasses specifically those environmental factors that would affect the relative reactivity of molecular trophic levels. The exact nature of the ζ function is unknown (here simulated as a first-order decay with increasing trophic level), but degradation probability is known to vary with location and environment (e.g. Hedges & Keil, 1995), and most diagenetic systems are treated using first-order decay approximations such as used here (e.g. Middelburg, 1989). Importantly, regardless of the form that ζ takes, in any given burial regime,

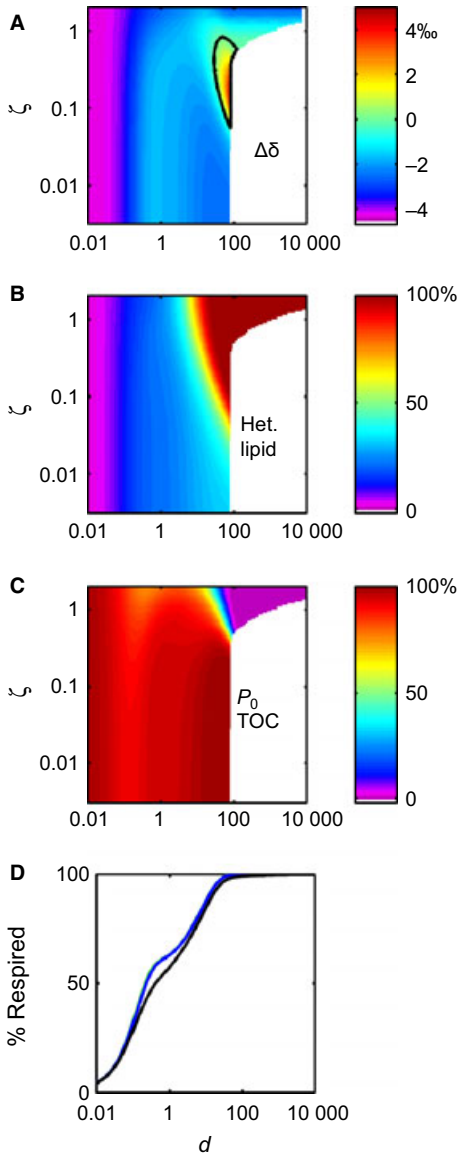

Fig. 3 Results of Logan-type scenario when exposure time is attenuated in higher trophic levels. (A) Dependence of $\Delta\delta_{n\text{-alkyl–TOC}}$ on overall degradation, *d*, and ζ, a scaling coefficient that determines the attenuation of degradation with increasing trophic level. The black contour follows a value of 0 for Δδ. (B) Contribution of heterotrophic lipid to total preserved lipid as a function of *d* and ζ. (C) Contribution of primary producers to total preserved TOC as a function of *d* and ζ. (D) Net respiration of primary productivity as a function of *d* and ζ (three overlapping colored lines show contrasting values).

only the *local* value of ζ would apply, and it is this value that would be reflected in the preserved value of $\Delta\delta_{n\text{-alkyl–TOC}}$.

In summary, under the heterotrophic enrichment scenario, there are two ways to produce sedimentary organic matter with a positive value of $\Delta\delta_{n\text{-alkyl–TOC}}$: (i) a specific relationship between ε_R, ε_L, b and E that also meets the unusual condition of $\varepsilon_R > \varepsilon_L$; or (ii) an 'optimum' diagenetic scenario, which can produce positive $\Delta\delta_{n\text{-alkyl–TOC}}$ over a narrow range of both exposure and attenuation (d and ζ).

While these conditions could exist in specific environmental settings, we believe that neither is a good candidate to be a controlling mechanism that would be fundamental to the entire Proterozoic, and yet would disappear unequivocally at the end of the eon. Option (ii) would be highly localized and would require specific burial scenarios. It is unreasonable to imagine that all depositional environments would be uniformly poised at attenuation coefficients (ζ) within the required, narrow range. Such environmental constancy appears to be refuted by the appearance of inverse isotopic signatures in samples from diverse water depths and environments, from evaporative carbonate platforms (Hieshima, 1992; Höld *et al.*, 1999) to deeper marine, shale-depositing environments (Logan *et al.*, 1997). In the case of option (i), there is no known mechanism for making recalcitrant molecules (algal biopolymers) and/or total kerogen that are systematically isotopically lighter than lipids. However, in some cases, ^{13}C-depleted kerogen has been attributed to the increased preservation of biomass from methanotrophic Archaea or Bacteria (e.g. Hinrichs, 2002; Eigenbrode *et al.*, 2008).

COMMUNITY HYPOTHESIS: ^{13}C DIFFERENCE BETWEEN PRIMARY PROKARYOTES AND EUKARYOTES

To consider an alternative to the Logan scenario, we examined the extent to which values of $\Delta\delta_{n\text{-alkyl–TOC}}$ could be controlled by the composition of the primary producer community. Presently, both eukaryotes and prokaryotes contribute to primary production in surface marine environments, but eukaryotes dominate primary biomass, C-fixation rate and even sometimes numerically (e.g. Agawin *et al.*, 2000). Although eukaryotic primary producers were present and active for several hundreds of millions of years prior to the Cambrian transition, they rose to global prominence in the latest Neoproterozoic and earliest Cambrian (e.g. Knoll *et al.*, 2007). This suggests that the total biomass attributable to prokaryotes and eukaryotes changed fundamentally across the end of the Proterozoic. If these biomass sources carried different ^{13}C signatures, this signal could have been transferred to sediments.

Size-population isotope model

In an ocean that contains prokaryotic (S, small) and eukaryotic (G, large) primary producers having different initial average ^{13}C contents, the isotopic signature of primary organic matter depends on the relative biomass ratios of these cell types in the surface ocean. Importantly, biomass ratios do not scale linearly with cell numbers, due to size:volume relationships. We treat the average size of S and G cells as the fractional radius of the small cells relative to the large cells ($R_z = r_S/r_G$). Similarly, the population of cells is treated as a ratio ($R_p = \text{cells}_S/\text{cells}_G$). We then model the total amount of biomass from a given cell type as $R_p R_z^3$, thereby assuming that the abundance of biomass in a cell is proportional to the cell volume and that the cells are spherical.

Relative ^{13}C enrichment in bacterial photoautotrophs has been observed in multiple taxa (Cyanobacteria, green and purple sulfur and non-sulfur bacteria; Pardue *et al.*, 1976; Sirevåg *et al.*, 1977; Roeske & O'Leary, 1985; Popp *et al.*, 1998; van Der Meer *et al.*, 2003) and modern aquatic environments (e.g. open marine: Tolosa *et al.*, 2008; Tchernov & Lipschultz, 2008; and lakes: Vuorio *et al.*, 2006; Gu & Schelske, 1996), and has been implicated in several geologic time periods (e.g. Miocene: Kashiyama *et al.*, 2008b; Cretaceous: Kashiyama *et al.*, 2008a; Sinninghe Damsté *et al.*, 2008; Jurassic: Schwab & Spangenberg, 2007; Permian: Grice *et al.*, 1996; Devonian: Joachimski *et al.*, 2001; Neoproterozoic: Riding, 2006). We model a community in which prokaryotic S primary producer cells are on average isotopically enriched compared to the larger G cells, and define β as the average net isotopic difference between the size classes. The ^{13}C content of large cells is defined as δ_{G_0}, and the starting ^{13}C content of small cells is $\delta_{S_0} = \delta_{G_0} + \beta$. Values of δ^{13}C of biochemical classes within the bulk S and G pools are offset by the biosynthetic fractionations ε_R and ε_L as described under the Logan scenario.

We formulate primary organic matter as a mixture of prokaryotic 'B' and 'L', and eukaryotic 'B', 'L' and 'R' (biochemical classes as in the Logan scenario). Although the resistant portion of biomass is prescribed for large cells only, it does not explicitly denote a biosynthetic class of material, but rather implies that resistance to degradation may be imparted due to mechanisms related to cell size, rather than specific chemical composition. Such mechanisms could include physical protection of eukaryotic biomass through cell-wall matrix effects (Nguyen *et al.*, 2003) or reduced exposure time via faster sinking through the water column (e.g. Burd & Jackson, 2009; Butterfield, 2009). Similarly, the model does not preclude the incorporation of prokaryotic (or eukaryotic) 'L' and 'B' into kerogen via geopolymerization. Degradation rates, heterotrophic uptake equations, and all other parameters are also formulated as described previously. Full details of derivations are given in Supporting Information.

Parameter values

To span a wide range of ecological space, we consider ratios of prokaryotic:eukaryotic cells from 10^1 to 10^7. In today's

ocean, more productive coastal and estuarine environments can have ratios $\sim 10^1$, while oligotrophic, subtropical ocean gyres have ratios $\sim 10^3$ (e.g. Hall & Vincent, 1990; Li, 1994; Fujieki *et al.*, 2010; Marañón *et al.*, 2010). We consider ranges of degradation extent, d, identical to those above, and the simulations are terminated as described previously. Attenuation of d with trophic level (ζ) is modeled for two values, $\zeta = 0$ (no attenuation) and $\zeta = 0.15$ (maximum effect on $\Delta\delta_{n\text{-alkyl–TOC}}$), for comparison to the Logan-type scenarios above.

Values for new parameters are shown in Table 2; all other model values were drawn from Table 1. We consider a conservative value of 4‰ for β, based on observations that Cyanobacteria could have values of $\delta^{13}C$ ~3–7‰ more positive relative to eukaryotes grown on the same C source (e.g. Popp *et al.*, 1998), whereas anoxygenic photoautotrophs using Type II Rubisco could have 6–9‰ enrichments (Roeske & O'Leary, 1985; Robinson & Cavanaugh, 1995), and those using the rTCA cycle could be >10‰ enriched (Sirevåg *et al.*, 1977; Preuß *et al.*, 1989; House *et al.*, 2003). Smaller kinetic isotope effects for their C-fixing enzymes and/or the use of carbon concentrating mechanisms (CCMs) could explain these ^{13}C enrichments (Erez *et al.*, 1998; Popp *et al.*, 1998; House *et al.*, 2003). Natural isotopic measurements of modern coexisting cyanobacteria and eukaryotic phytoplankton are sparse, and use varying methods to separate size classes and/or individual taxa. Resulting measurements correspond to a wide range of β values if comparison between individual taxa of cyanobacteria and eukaryotes was considered (−9 to +19; Gu & Schelske, 1996; Vuorio *et al.*, 2006; Tolosa *et al.*, 2008). This sort of variability is also reflected in culture studies (Pardue *et al.*, 1976; Falkowski, 1991). However, since we are considering what would constitute a weighted average of values across a diverse marine population, we confine our simulations to a more modest range of β.

To model cell sizes, we assume that average marine bacteria are 0.8 μm in diameter and use an R_z of 1/15, resulting in eukaryotic algae smaller than present-day coccolithophorids. This yields a conservative estimate of the contrast in size between cell types. Notably, due to this choice of R_z, primary biomass ratios for S:G are 1:1 when $R_p \sim 10^{3.5}$. In other words, biomass dominance of eukaryotes appears when S:G is $<\sim 10^{3.5}$ or disappears when S:G > $\sim 10^{3.5}$; the latter would be only slightly higher than modern, oligotrophic gyres. Finally, we consider the proportions of 'B' and 'L' in primary prokaryotes to be the same as in heterotrophic prokaryotes.

Table 2 Additional model parameters and values, mixed community scenario

Additional parameters, Mixed community model	Symbol	Value used in examples	Range for Monte Carlo
Difference in $\delta^{13}C$ value average biomass, small cells–large	β	4‰	0–8‰
Radius size ratio, small/large cells	R_z	1/15	Fixed
Fraction labile biomass, primary small cells	F_{SB}	90%	75–95%
			$(1 - F_{SL})$
Fraction lipid, primary small cells	F_{SL}	10%	5–25%

Results of size-fractionated scenarios

The size-fractionated biomass model (Fig. 4) was tested by varying the numerical ratio of small:large cells and the total extent of degradation. A positive value for $\Delta\delta_{n\text{-alkyl–TOC}}$ requires that sedimentary lipid must be dominated by input from S cells and/or heterotrophs, while most sedimentary TOC must originate from G cells. The areas producing positive values of Δδ in Fig. 4A,F correspond to an intermediate contribution of preserved lipid from S cells (Fig. 4B,G), coincident with an intermediate contribution of preserved TOC from G cells (Fig. 4D,I).

A positive value of $\Delta\delta_{n\text{-alkyl–TOC}}$ (Fig. 4A,F) is relatively insensitive to the contribution of heterotrophs to preserved lipid (Fig. 4C,H). The relative contribution of heterotrophic lipids to a positive Δδ signal is smaller than in the Logan scenarios, because the lipids of heterotrophs and of S cells both are ^{13}C-enriched. The lipids of heterotrophs become significantly abundant only when the upper limit of d is simultaneous with $\zeta > 0$ (Fig. 4H). This results from extensive degradation of S lipids from trophic level 0, while heterotrophic lipids in trophic level N can accumulate. In the example shown here, the additional heterotrophic contribution causes maximum values for Δδ to become slightly more positive (from ~1.2‰ in Fig. 4A to ~2.6‰ in Fig. 4F).

Thus, although the maximum value of $\Delta\delta_{n\text{-alkyl–TOC}}$ is governed by the contribution of preserved heterotrophic lipids, this effect occurs over a small range of d. The majority of positive Δδ space (Fig. 4A,F) is governed by the differential preservation of components of S and G cells. The absolute value of Δδ depends on our choice of β, specifically in relation to the biosynthetic fractionations prescribed for ε_R and ε_L. In the extreme case of sedimentary lipid contributed *only* by small cells and TOC *only* by large cells, the *maximum* value of Δδ would be equal to $\delta_{SL} - \delta_{GR}$, which reduces to $\varepsilon_R + \beta - \varepsilon_L$, or 1‰ using values from Tables 1 and 2. The larger expressed maximum of ~1.2‰ (Fig. 4A) is due to a non-zero contribution of heterotrophic lipids slightly overwhelming a small, but continued presence of lipid from ^{13}C-depleted G cells. Accordingly, the Δδ signature more readily stays positive once a large enough ratio of small:large cells is achieved, as δ_{SL} (plus heterotrophic lipids) dominates the total δ_L. Under conditions of very high ratios of S:G, however, there no longer is enough biomass from G to contribute to TOC. Both the total δ_L and δ_{TOC} are dominated by material from S cells and the positive signature for Δδ decreases. When population ratios change in the other direction, the positive signal in Δδ disappears rapidly and completely when S:G falls below $\sim 10^{3.5}$.

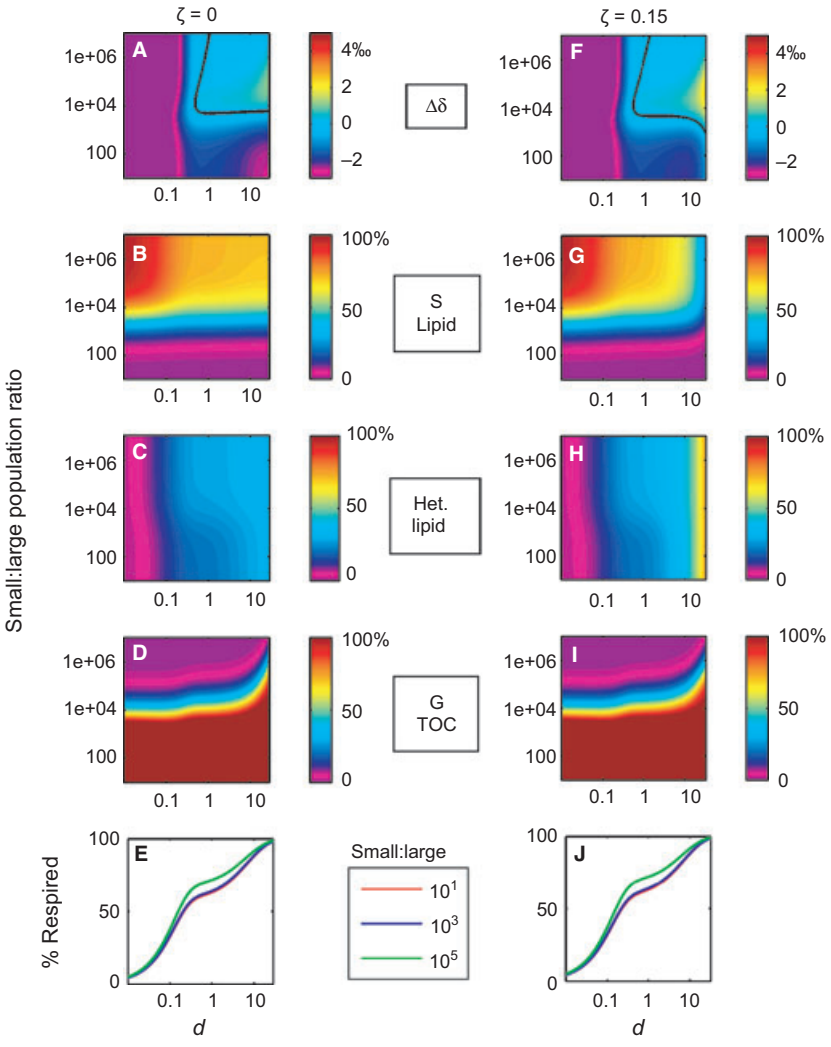

Fig. 4 Results of mixed community scenario. The ζ = 0 case (A–E) indicates results when *d* remains constant for all trophic levels; the ζ = 0.15 case (F–J) is shown for comparison to the Logan scenarios, in which *d* is attenuated at higher trophic levels. (A,F) Dependence of $\Delta\delta_{n\text{-alkyl–TOC}}$ on overall degradation, *d*, and population ratio of small(S):large(G) primary producer cells (R_P). The black contour follows a value of 0 for Δδ. (B,G) Contribution of lipid from primary S cells to total preserved lipid as a function of *d* and R_P. (C,H) Contribution of heterotrophic lipid to total preserved lipid as a function of *d* and R_P. (D,I) Contribution of primary G cells to total preserved TOC as a function of *d* and R_P. (E,J) Net respiration of primary productivity as a function of *d* for several different R_P shows convergence of all models at high *d*, regardless of ζ. Contour values in (B,C,G,H) are % of total lipid; in (D,I) are % of TOC.

COMPARISON TO INVERSE $\Delta\delta^{13}C_{N\text{-ALKYL–ISOPRENOID}}$

Additional studies have reported the inverse pattern by comparing the isotopic content of selected *n*-alkyl lipids to the isoprenoid lipids pristane and phytane. The latter represent photosynthetic sources as they are thought to derive mostly from chlorophyll *a* (Logan *et al.*, 1995, 1997; Kelly, 2009). The measured $\Delta\delta_{n\text{-alkyl–isoprenoid}}$ offset most commonly varies in magnitude from ~0‰ to 4‰ (Logan *et al.*, 1995, 1997; Kelly, 2009), although larger offsets have been reported for one Cryogenian horizon (Kelly, 2009).

In samples in which inverse signatures are observed in both $\Delta\delta_{n\text{-alkyl–kerogen}}$ and $\Delta\delta_{n\text{-alkyl–isoprenoid}}$, the isotopic ordering between isoprenoids and kerogen is variable, covering both positive and negative values (Fig. 1) (Logan *et al.*, 1995, 1997). This variability has been attributed to an archaeal contribution to the pool of phytane (Logan *et al.*, 1997; Schouten *et al.*, 1998), and the relative effect has been estimated by assuming that Archaea are responsible for any inconsistency in the pristane to phytane abundance ratio or isotopic values (Logan *et al.*, 1997). However, there are other ways to generate variability in $\Delta\delta_{n\text{-alkyl–isoprenoid}}$ that do not require the presence of Archaea.

To demonstrate this, we incorporated an isoprenoid component into both the Logan scenario and the mixed community scenario. We assume that pristane and phytane are from photosynthetic sources only, that their abundance is proportional to the biomass in photosynthetic cells (both S and G), and that they are biosynthesized with an average fractionation $\varepsilon_{\text{biomass–isoprenoid}}$ of 3‰ for plastidic lipids (e.g. Schouten *et al.*, 1998; Hayes, 2001).

When *d* is not attenuated by trophic level (ζ = 0), values for $\delta_{\text{isoprenoid}}$ and for $\delta_{n\text{-alkyl}}$ change in parallel, and the difference between them ($\Delta\delta_{n\text{-alkyl–isoprenoid}}$) must remain equal to the difference expected for biosynthetic control (−1.5‰). It is not possible to make the sign or magnitude of this relationship change unless a non-zero value of ζ is incorporated.

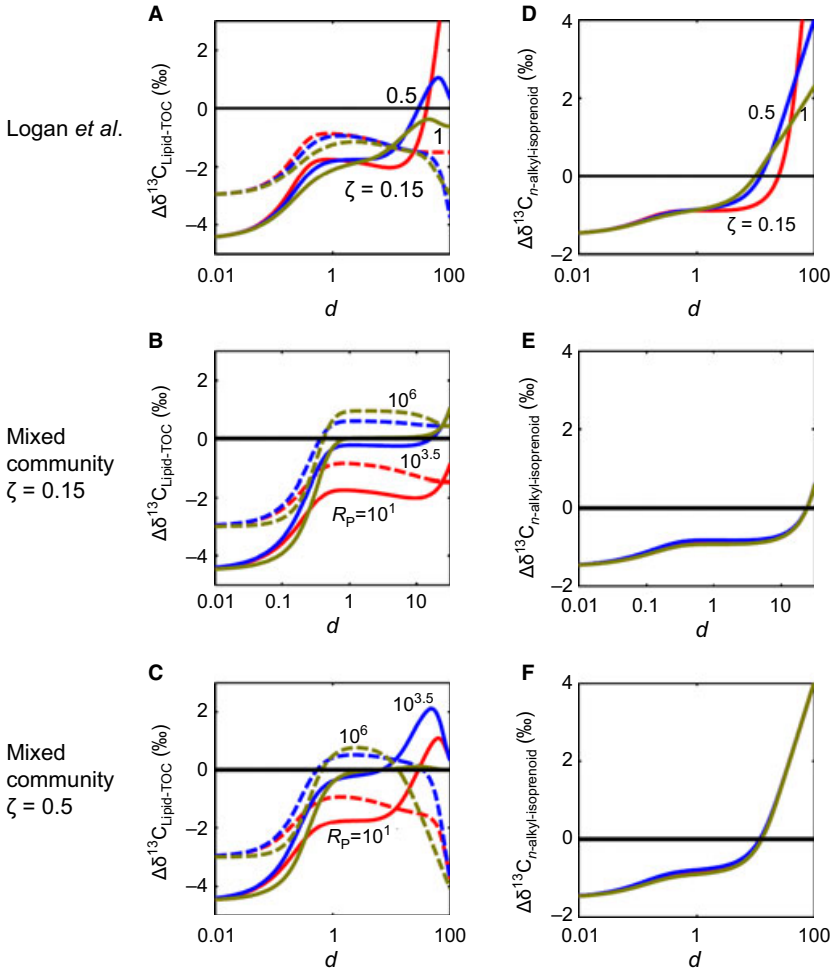

Fig. 5 Modeled $\Delta\delta_{n\text{-alkyl–isoprenoid}}$ isotope anomalies for the Logan scenario (A,D) and mixed community scenario at ζ = 0.15 (B,E) and at ζ = 0.5 (C,F). Relative isotope anomalies are shown for isoprenoid (dashed) and *n*-alkyl (solid) lipids, each normalized to TOC (black line at 0‰). Colors illustrate results with three different values for the controlling parameter in each scenario (low to high: red, blue, green): ζ, trophic attenuation factor (A,D); and R_P, population ratio of primary small cells to large cells (B,E,C,F). In the left-hand column, values above zero indicate an inverse signature for $\Delta\delta_{n\text{-alkyl–TOC}}$ and $\Delta\delta_{isoprenoid\text{–TOC}}$; in the right-hand column, values above zero indicate an inverse signature for $\Delta\delta_{n\text{-alkyl–isoprenoid}}$.

Therefore, values of $\Delta\delta_{n\text{-alkyl–TOC}}$ and $\Delta\delta_{n\text{-alkyl–isoprenoid}}$ were modeled for the Logan scenario at three different values of ζ (Fig. 5A,D) and for the mixed community scenario at three different population ratios R_P and two different ζ (Fig. 5B,E,C,F). At low *d* in all scenarios, the relationship between isoprenoids and *n*-alkyl lipids continues to reflect that of biosynthetic products (Fig. 5), but at higher *d*, values of $\Delta\delta_{n\text{-alkyl–isoprenoid}}$ become positive in all models (Fig. 5D–F).

The mixed community scenario produces a positive $\Delta\delta_{n\text{-alkyl–isoprenoid}}$ signature for values of ζ >0.125 and moderate to high values of *d*. Figure 5(B,E) is shown at ζ = 0.15, the value at which maximum $\Delta\delta_{n\text{-alkyl–TOC}}$ is obtained in the Logan scenario; Fig. 5C,F is shown at ζ = 0.5, a value that illustrates a wide range of isotopically positive values for both types of lipids.

At elevated ζ, a changing population ratio R_P can reproduce the variability seen in the isotopic relationship between preserved isoprenoids and kerogen (Fig. 1B), with both positive and negative offsets occurring in conjunction with positive values of $\Delta\delta_{n\text{-alkyl–TOC}}$ and $\Delta\delta_{n\text{-alkyl–isoprenoid}}$. In a modestly prokaryotic ocean (blue line; Fig. 5C,F), between $\sim 10 < d < 40$ (degradational extents from ~85% to 99%), $\Delta\delta_{n\text{-alkyl–TOC}}$, $\Delta\delta_{n\text{-alkyl–isoprenoid}}$ and $\Delta\delta_{isoprenoid\text{–TOC}}$ all are positive, as seen throughout many Proterozic samples. Approaching maximum *d*, however, $\Delta\delta_{n\text{-alkyl–isoprenoid}}$ remains positive (Fig. 5F), whereas $\Delta\delta_{isoprenoid\text{–TOC}}$ returns to a negative (biosynthetic) value.

Importantly, these models can simulate some unusual data from the Cambrian. Continued positive values for $\Delta\delta_{n\text{-alkyl–isoprenoid}}$ occur in the early Cambrian, but they are found alongside negative values for $\Delta\delta_{n\text{-alkyl–kerogen}}$ (Logan *et al.*, 1997). Both the Logan scenario and the mixed community scenario can reproduce this effect. In the Logan scenario, $\delta_{n\text{-alkyl}}$ is more positive than $\delta_{isoprenoid}$ at high values of *d* and ζ, although both are negative relative to δ_{TOC} (Fig. 5A). In the mixed community scenario at ζ = 0.15, $\delta_{n\text{-alkyl}}$ is more positive than $\delta_{isoprenoid}$ at high values of *d* and moderate values of R_P, but $\delta_{n\text{-alkyl}}$ can be negative relative to δ_{TOC} if R_P decreases (eukaryotes become more abundant; Fig. 5B). Still another Cambrian formation (Observatory Hills; Logan *et al.*, 1997) shows Phanerozoic (biosynthetic) patterns by having negative

values of $\Delta\delta_{n\text{-alkyl–isoprenoid}}$ (isoprenoids heavier than *n*-alkyl lipids) and negative values of $\Delta\delta_{n\text{-alkyl–kerogen}}$ (kerogen heavier than *n*-alkyl lipids), but positive values for isoprenoids in relation to kerogen. This pattern can be reproduced in the community mixing model at moderate values of *d* (Fig. 5B,C), but not in the Logan model (Fig. 5A).

DISCUSSION

Uncertainty in and sensitivity to parameter values

Most of the parameters in our models have wide ranges of values in the current literature. Properties of water column and sedimentary environments, as well as cell physiologies and phylogenies, remain relatively unknown for the Proterozoic. We have attempted to account for this large range of uncertainty by choosing parameter values conservatively, erring on the side of values that favor success of a Logan-type model, rather than the community model. Our relative results are thus significant, whereas the absolute values are highly dependent on the inputs. Figure 6 shows the frequency distribution of results that successfully display a positive value for $\Delta\delta_{n\text{-alkyl–TOC}}$ in a Monte Carlo simulation designed to explore the sensitivities of both models. Parameter values and combinations were chosen at random for each of $>6 \times 10^6$ simulations. Ranges of values used for these Monte Carlo simulations are shown in Tables 1 and 2 and are discussed further in the Supporting Information.

The frequency distribution of positive $\Delta\delta_{n\text{-alkyl–TOC}}$ in Fig. 6 is similar to the patterns shown in Figs 3 and 4. This indicates that the variables shown in Figs 3 and 4 are indeed the ones to which the models are most sensitive. In all cases, however, the range that results in an inverse signature is expanded in Fig. 6. It remains true that in the Logan case the bulk of inverse results occur within a small range of high *d* surrounding an intermediate ζ (Fig. 6A). These variables clearly are interrelated conceptually, as extensive later-stage heterotrophy necessarily occurs only when the total degradation of primary organic matter is high. The fact that the mixed community scenario also shows a stronger dependency on *d* when a non-zero value of ζ is incorporated (Fig. 6C) also highlights this connection.

The mixed community scenario is otherwise more dependent on other parameter combinations. It produces a broader range of positive results for $\Delta\delta_{n\text{-alkyl–TOC}}$ across a wider range of ζ, including at ζ = 0 (Fig. 6B). The major driver of the magnitude of Δδ is of course β, which is the ultimate determinant of isotopic enrichment in a non-eukaryotic source of *n*-alkyl lipids. Although positive values of Δδ also are driven by the small:large population ratio and *d*, specific combinations of these variables alone do not *guarantee* an inverse outcome, especially when ζ = 0 (Fig. 6B; no cases of 100% success) due to our incorporation of a range of β values. Dependence of

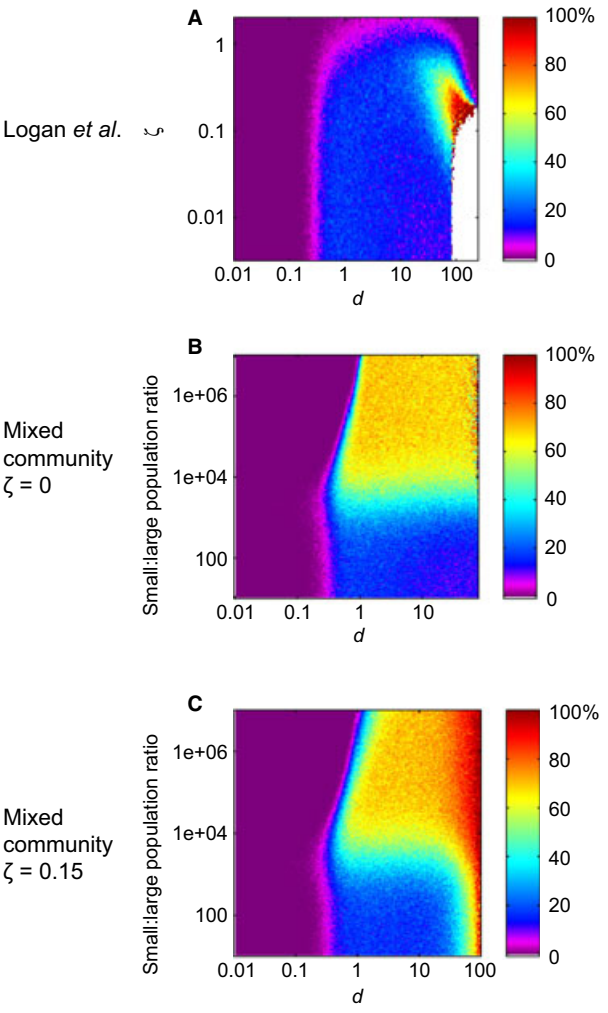

Fig. 6 Results of $>6 \times 10^6$ Monte Carlo simulations, drawing from parameter ranges in Tables 1 and 2. Color map indicates percentage of simulations resulting in an inverse (>0‰) value for $\Delta\delta_{n\text{-alkyl–TOC}}$. Results for the Logan scenario (A) are shown for varying *d* and ζ and have been limited to *d* values displaying non-zero outcomes, up to $10^{2.5}$. Results are shown for the mixed community scenario for varying *d* and R_P, and both for when ζ = 0 (B) and ζ = 0.15 (C).

inverse results on the value for β is shown in Fig. 7, which indicates that values of β as low as 3‰ still produce positive values of Δδ in >40% of trials.

Comparison of models to the Proterozoic environment

The measured inverse signature of $\Delta\delta_{n\text{-alkyl–kerogen}}$ during the Proterozoic manifests as a general trend across a large global extent of shelf and outer shelf–slope facies. While the magnitude of the signature is somewhat variable, the positive sign is almost exclusive to the Precambrian, with a trend toward negative values starting in the latest Ediacaran–early Cambrian (Logan *et al.*, 1995, 1997). The Proterozoic was a time of enormous change in global biogeochemical cycles (e.g. Canfield, 1998; Anbar & Knoll, 2002; Johnston *et al.*, 2009).

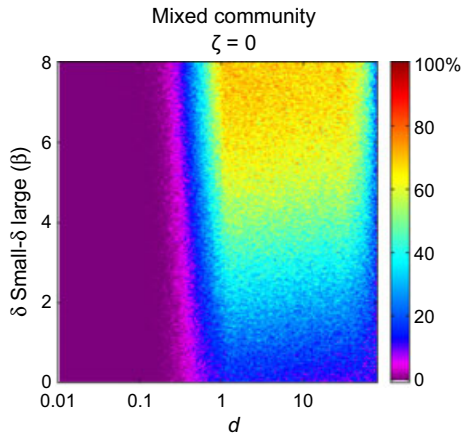

Fig. 7 Results of >6 × 10^6 Monte Carlo simulations, drawing from parameter ranges in Tables 1 and 2. Color map indicates percentage of simulations resulting in an inverse (>0‰) value for $\Delta\delta_{n\text{-alkyl–TOC}}$. Explicit dependency on d and β is shown; all other parameters were randomized. Results are shown for the mixed community scenario with ζ = 0.

Marine biogeochemistry was probably controlled by variability in oxygen concentrations and changes in the sulfur cycle (e.g. Fike *et al.*, 2006), and the redox environments in different parts of the ocean supported different populations and likely differing rates of diagenesis (e.g. Logan *et al.*, 1999; Canfield *et al.*, 2008; McFadden *et al.*, 2008). Despite this potential for redox heterogeneity, the inverse signature of $\Delta\delta_{n\text{-alkyl–kerogen}}$ remained ubiquitous, suggesting that it derived from environmental or ecological conditions that were fundamental to the entire era.

In our formalization of the Logan hypothesis, a ubiquitous inverse signature would derive from consistently very high exposure to degradation (d) for primary organic matter, and intermediate levels of attenuation of this exposure for heterotrophs (ζ), across most preserved environments. Magnitudes of the Δδ signature could then vary widely within the narrow range of allowed d and ζ (Fig. 3). While water-column degradation could be enhanced due to slower sinking rates of photosynthetic cells (e.g. Logan *et al.*, 1995; Butterfield, 2009), total respiration may have been limited by low oxidant availability. Therefore, explanations *requiring* very high values of d might not be expected to apply ubiquitously throughout the eon. But supposing that environmental conditions did impose a strictly high d, then the switch to a negative value of $\Delta\delta_{n\text{-alkyl–kerogen}}$ mostly likely would derive from a gradual relaxation of the conditions that caused a fixed value of ζ. The questions then are how could a narrow control on ζ be maintained, and how would it be universally relaxed in the latest Ediacaran? It is difficult to envision how attenuation of degradation would have been uniformly constant during the Proterozoic. The parameter ζ is presumed to integrate many environmental factors such as particle sinking rate and variability in exposure to oxidants. Considering the likely heterogeneity of degradative conditions across the Proterozoic, a consistently narrow range of net ζ appears to be an unreasonably strict requirement. The eventual change in ζ potentially could be related to an increased sinking flux for primary producers, possibly as a result of increased biomineralization. However, inorganic ballast during the Proterozoic has been suggested to be abundant enough to cause high organic burial rates (e.g. Hotinski *et al.*, 2004), and modern microbially dominated ecosystems are capable of sustaining significant export of primary organic matter (e.g. Hotinski *et al.*, 2004; Richardson & Jackson, 2007). This suggests that increased sinking particle sizes in the early Cambrian may not have altered the preservation mechanisms sufficiently to produce a monotonic shift in $\Delta\delta_{n\text{-alkyl–kerogen}}$.

Positive values of $\Delta\delta_{n\text{-alkyl–kerogen}}$ across diverse diagenetic histories are accommodated more easily by a mechanism that allows a wider range of total degradation (d), and allows but does not require an attenuation factor (ζ). The mixed community model satisfies these requirements. In the mixed community scenario, a ubiquitous positive value of $\Delta\delta_{n\text{-alkyl–kerogen}}$ would result from a relatively high ratio of ^{13}C-enriched prokaryotic production and variably intermediate to high extent of d. Meanwhile, ζ could be ≥0 and could be permitted to vary over a wide range. This scenario accommodates redox heterogeneity and would allow the positive isotope signal to be observed in a variety of marine facies. There is no requirement for selective preservation of heterotrophic biomass. Variability in the predicted magnitude of $\Delta\delta_{n\text{-alkyl–kerogen}}$ is somewhat smaller in the mixed community model, but the range of population ratios for which an inverse signature is retained is large. The switch to a negative sign of Δδ in the late Ediacaran would signal a fundamental ecological transition in response to geochemical changes favoring the gradual increase in eukaryotic proportion of primary production over time.

The trend of measured values for $\Delta\delta_{n\text{-alkyl–isoprenoid}}$ in the Proterozoic is similar to that for $\Delta\delta_{n\text{-alkyl–kerogen}}$, but with relatively more outliers, a wider range of magnitudes in some sections, and several measurements of continued inverse signatures in the Cambrian (Logan *et al.*, 1995, 1997; Kelly, 2009). A non-zero value of ζ is required to produce an inverse $\Delta\delta_{n\text{-alkyl–isoprenoid}}$ in both models, and variability in d at a given ζ can reproduce the observed variability in $\Delta\delta_{n\text{-alkyl–isoprenoid}}$. However, only the mixed community scenario is capable of simulating the full range of simultaneous combinations of sign relationships observed for $\Delta\delta_{n\text{-alkyl–TOC}}$, $\Delta\delta_{n\text{-alkyl–isoprenoid}}$ and $\Delta\delta_{\text{isoprenoid–TOC}}$. The overall heterogeneity of the observational data may then be a consequence of heterogeneity in both environmental and ecological parameters. A purely heterotrophy-based model like the Logan scenario is unable to reproduce the same diversity of signatures, and in general is less accommodating of a variable environment in its requirements for creating inverse isotopic signatures.

Our model addresses a conservative formulation of organic matter production and biosynthetic isotope patterns for the Proterozoic, but there are additional mechanisms by which

preserved *n*-alkyl lipids could acquire relative ^{13}C enrichment. Most simply, some photoautotrophs during the Proterozoic could have had different pathways of lipid biosynthesis that result in an 'inverse' isotopic ordering of their direct biosynthetic products, as seen in rTCA organisms (van Der Meer *et al.*, 1998). A second way would be for the isotopically enriched portion of the community (whether primary or heterotrophic) to have a relatively high cellular lipid content compared to other organisms, thereby contributing disproportionate quantities of ^{13}C-enriched lipids to the sedimentary pool (as suggested for inverse isotope ordering in the Archean; Brocks *et al.*, 2003b). Finally, inverse $\Delta\delta_{n\text{-alkyl–isoprenoid}}$ values specifically could arise from our model without invoking $\zeta > 0$, if the predominant isotopically enriched photoautrophs had a chlorophyll side-chain based on farnesene, i.e. not contributing to pristane and phytane. Although likely present to some extent in the Proterozoic, these alternative mechanisms are difficult to invoke as controlling factors across all environments spanning the entire eon. Our model is able to show that none of these mechanisms is *necessary* to explain inverse $\Delta\delta$; including some proportion of organisms producing these alternative effects simply would widen the parameter range under which our model produces inverse signatures.

The value chosen for β in our model may err on the side of conservative: Proterozoic ocean conditions may have promoted ^{13}C depletion in eukaryotes while favoring photosynthetic prokaryotes that tend to discriminate less against ^{13}C. While the proportional significance of prokaryotic oxygenic and anoxygenic photoautotrophs remains largely unknown for the Proterozoic (e.g. Eigenbrode & Freeman, 2006; Johnston *et al.*, 2009), both are expected to have discriminated less against ^{13}C than photosynthetic eukaryotes (e.g. Schidlowski, 1987; Badger & Price, 2003; Riding, 2006). Modern prokaryote-dominated areas of the open ocean may provide our closest observable analog to likely conditions that persisted in the Proterozoic. Prokaryotic autotrophy currently dominates some tropical, oligotrophic marine settings (Agawin *et al.*, 2000), where small cell size is likely to impart fundamental physiological advantages (e.g. Raven, 1998; Jiang *et al.*, 2005). Contemporary evidence suggests that in these environments, Cyanobacteria are likely to be enriched in ^{13}C relative to coexisting eukaryotic producers (e.g. Popp *et al.*, 1998; Tolosa *et al.*, 2008). Cyanobacteria are suspected to operate CCMs obligately in modern natural settings, and also use them constitutively under high CO_2 conditions (Price *et al.*, 1998). Colonial behavior can also impose local CO_2 limitation, depressing the expressed ^{13}C fractionation in biomass due to the activity of CCMs (Pardue *et al.*, 1976; Tchernov & Lipschultz, 2008).

Although the environmental controls on the expression of ^{13}C discrimination in eukaryotic Rubisco are complex, low growth-rates and/or high CO_2 availability lead to expression of near-maximum fractionation factors in C-fixation in eukaryotic cells (e.g. Popp *et al.*, 1998); both of these conditions likely were favored in Proterozoic oceans. Smaller average cell size of eukaryotic phytoplankton also was likely in the Proterozoic, as is favored in modern oligotrophic environments. The corresponding high surface area would tend to increase CO_2 diffusion into the cell (e.g. Raven, 1998). All of these factors would contribute to ^{13}C-depletion in eukaryotes. Together the prokaryotic and eukaryotic effects could increase the magnitude of β.

Modern observational data support these suggestions. Recent measurements from the Central North Pacific gyre show that ^{13}C-enriched lipids are found among the small size class (0.2–0.5 μm organic matter) and might be abundantly exported to mesopelagic depths (Close *et al.*, unpubl. data). Compound-specific isotopic measurements on oligotrophic water-column filtrates and on sediments recovered from deep-sea cores could help expand our understanding of prokaryote-dominated marine environments and provide valuable analogs to the Proterozoic.

Relative biomarker abundances also may be valuable tools to elucidate populations contributing to inverse isotope signatures. For instance, biomarkers for anoxygenic photosynthesizing bacteria can be helpful in conceptualizing possible sources of organic matter in a mixed phytoplankton community and the isotopic consequences for TOC and/or individual compounds (e.g. Hollander *et al.*, 1993; Schwab & Spangenberg, 2007). Sedimentary hopane:sterane ratios also are frequently interpreted to indicate the possible relative contribution of bacteria (photosynthetic or heterotrophic) to sedimentary organic matter. Given the results of the mixed community model as shown in Fig. 4, inverse values of $\Delta\delta_{n\text{-alkyl–TOC}}$ are achieved at a population ratio of primary prokaryotes:eukaryotes $\geq\sim 10^{3.5}$. This corresponds to biomass ratios of $\geq\sim$1:1. Making the very broad assumptions that hopanes and steranes comprise approximately equal fractions of the biomass of their respective sources and that they degrade at rates proportional to *n*-alkyl lipids, hopane:sterane ratios could be ~1:1, even when the $\Delta\delta_{n\text{-alkyl–TOC}}$ signature is still positive. This is consistent with observations from the Proterozoic (Grosjean *et al.*, 2009; Love *et al.*, 2009). Accordingly, the transition of the $\Delta\delta$ signature to negative values need not accompany a major disturbance in the biomarker record. Given the many uncertainties in translating biomarker ratios to quantitative estimates of the associated biomass, this supports the idea that such ratios benefit from concomitant isotopic measurements.

CONCLUSIONS

It has been suggested previously that ^{13}C-enriched lipids in Proterozoic and Archean deposits could derive from a distinct portion of the photosynthetic community (Hieshima, 1992; Logan *et al.*, 1997; Brocks *et al.*, 2003b), but until now this idea has not been explored quantitatively or adopted as an

explanation for Proterozoic inverse organic isotopic patterns. Conversely, the suggestion that ^{13}C-enriched lipids derive from preferentially preserved late-stage heterotrophs (Logan *et al.*, 1995) has been widely adopted, but to date the potential mechanisms for this effect have not been treated quantitatively. Our models support the former idea.

Consistent inverse values for $\Delta\delta_{n\text{-alkyl–kerogen}}$ are most easily and broadly explained by an isotopically heterogeneous community of primary producers, and not solely by preferential preservation of lipids from heterotrophs. However, inverse values observed for $\Delta\delta_{n\text{-alkyl–isoprenoid}}$ are best explained in the model by enhanced preservation of heterotrophs *within* a mixed primary community scenario. The latter signature implicates the importance of non-uniform degradation as a function of trophic level. In turn, this suggests that variations in environment-specific factors like stratification, water depth and oxygen concentrations are more readily expressed within the $\Delta\delta_{n\text{-alkyl–isoprenoid}}$ signal; while the overall fractionations between organic and inorganic carbon are best represented by *n*-alkyl lipids, kerogen and carbonate. More compound-specific isotopic measurements from all time periods of the Proterozoic and Cambrian – from well-constrained environmental settings – should help to elucidate more detailed controls on these signatures.

ACKNOWLEDGMENTS

We would like to thank Dan Rothman, Roger Summons, Alex Bradley and John Hayes for helpful discussions; and Rita Parai for Matlab advice. This work was supported by an Exxon Mobil Geoscience Grant (to H.G.C.), the Harvard University Science and Engineering Committee (HUSEC), and by NSF-OCE-0927290 and the David and Lucille Packard Foundation (to A.P.). We also thank Lee Kump for editorial assistance and four anonymous referees for their valuable comments.

REFERENCES

Agawin NSR, Duarte CM, Agustí S (2000) Nutrient and temperature control of the contribution of picoplankton to phytoplankton biomass and production. *Limnology and Oceanography* **45**, 591–600.

Allard B, Templier J, Largeau C (1997) Artifactual origin of mycobacterial bacteran. Formation of melanoidin-like artifact macromolecular material during the usual isolation process. *Organic Geochemistry* **26**, 691–703.

Anbar A, Knoll A (2002) Proterozoic ocean chemistry and evolution: a bioinorganic bridge? *Science* **297**, 1137–1142.

Badger MR, Price GD (2003) CO_2 concentrating mechanisms in cyanobacteria: molecular components, their diversity and evolution. *Journal of Experimental Botany* **54**, 609–622.

Brocks JJ, Buick R, Logan Ga, Summons RE (2003a) Composition and syngeneity of molecular fossils from the 2.78 to 2.45 billion-year-old Mount Bruce Supergroup, Pilbara Craton, Western Australia. *Geochimica et Cosmochimica Acta* **67**, 4289–4319.

Brocks JJ, Buick R, Summons RE, Logan GA (2003b) A reconstruction of Archean biological diversity based on molecular fossils from the 2.78 to 2.45 billion-year-old Mount Bruce Supergroup, Hamersley Basin, Western Australia. *Geochimica et Cosmochimica Acta* **67**, 4321–4335.

Burd AB, Jackson GA (2009) Particle aggregation. *Annual Review of Marine Science* **1**, 65–90.

Butterfield NJ (2009) Oxygen, animals and oceanic ventilation: an alternative view. *Geobiology* **7**, 1–7.

Canfield D (1998) A new model for Proterozoic ocean chemistry. *Nature* **396**, 450–453.

Canfield D, Poulton SW, Knoll AH, Narbonne GM, Ross G, Goldberg T, Strauss H (2008) Ferruginous conditions dominated later Neoproterozoic deep-water chemistry. *Science* **321**, 949–952.

Dawson D, Grice K, Alexander R, Edwards D (2007) The effect of source and maturity on the stable isotopic compositions of individual hydrocarbons in sediments and crude oils from the Vulcan Sub-basin, Timor Sea, Northern Australia. *Organic Geochemistry* **38**, 1015–1038.

DeNiro M, Epstein S (1978) Influence of diet on the distribution of carbon isotopes in animals. *Geochimica et Cosmochimica Acta* **42**, 495–506.

van Der Meer MTJ, Schouten S, Sinninghe Damsté JS (1998) The effect of the reversed tricarboxylic acid cycle on the ^{13}C contents of bacterial lipids. *Organic Geochemistry* **28**, 527–533.

van Der Meer MTJ, Schouten S, Sinninghe Damsté JS, de Leeuw JW, Ward DM (2003) Compound-specific isotopic fractionation patterns suggest different carbon metabolisms among Chloroflexus-like bacteria in hot-spring microbial mats. *Applied and Environmental Microbiology* **69**, 6000–6006.

Eigenbrode JL, Freeman KH (2006) Late Archean rise of aerobic microbial ecosystems. *Proceedings of the National Academy of Sciences of the USA* **103**, 15759–15764.

Eigenbrode J, Freeman K, Summons R (2008) Methylhopane biomarker hydrocarbons in Hamersley Province sediments provide evidence for Neoarchean aerobiosis. *Earth and Planetary Science Letters* **273**, 323–331.

Erez J, Bouevitch A, Kaplan A (1998) Carbon isotope fractionation by photosynthetic aquatic microorganisms: experiments with Synechococcus PCC7942, and a simple carbon flux model. *Canadian Journal of Botany* **76**, 1109–1118.

Falkowski PG (1991) Species variability in the fractionation of ^{13}C and ^{12}C by marine phytoplankton. *Journal of Plankton Research* **13**, 21–28.

Fike DA, Grotzinger JP, Pratt LM, Summons RE (2006) Oxidation of the Ediacaran ocean. *Nature* **444**, 744–747.

Fujieki L, Santiago-Mandujano F, Lethaby P, Lukas R, Karl D (2010) *Hawaii Ocean Time-Series Program Data Report 19: 2007.* University of Hawaii School of Ocean and Earth Science and Technology, Honolulu, HI, 403 pp. Available at: http://hahana.soest.hawaii.edu/hot/reports/reports.html.

del Giorgio P, Cole J (1998) Bacterial growth efficiency in natural aquatic systems. *Annual Review of Ecology and Systematics* **29**, 503–541.

Grice K, Schaeffer P, Schwark L, Maxwell JR (1996) Molecular indicators of palaeoenvironmental conditions in an immature Permian shale (Kupferschiefer, Lower Rhine Basin, north-west Germany) from free and S-bound lipids. *Organic Geochemistry* **25**, 131–147.

Grice K, Cao C, Love GD, Böttcher ME, Twitchett RJ, Grosjean E, Summons RE, Turgeon SC, Dunning W, Jin Y (2005) Photic zone euxinia during the Permian-Triassic superanoxic event. *Science* **307**, 706–709.

Grosjean E, Love GD, Stalvies C, Fike DA, Summons RE (2009) Origin of petroleum in the Neoproterozoic–Cambrian South Oman Salt Basin. *Organic Geochemistry* **40**, 87–110.

Grossi V, Blokker P, Sinninghe Damsté JS (2001) Anaerobic biodegradation of lipids of the marine microalga Nannochloropsis salina. *Organic Geochemistry* **32**, 795–808.

Gu B, Schelske CL (1996) Temporal and spatial variations in phytoplankton carbon isotopes in a polymictic subtropical lake. *Journal of Plankton Research* **18**, 2081–2092.

Guthrie JM (1996) Molecular and carbon isotopic analysis of individual biological markers: evidence for sources of organic matter and paleoenvironmental conditions in the Upper Ordovician Maquoketa Group, Illinois Basin, U.S.A. *Organic Geochemistry* **25**, 439–460.

Hall J, Vincent W (1990) Vertical and horizontal structure in the picoplankton communities of a coastal upwelling system. *Marine Biology* **106**, 465–471.

Hartnett H, Keil R, Hedges J, Devol A (1998) Influence of oxygen exposure time on organic carbon preservation in continental margin sediments. *Nature* **391**, 2–4.

Harvey HR, Macko SA (1997) Catalysts or contributors? Tracking bacterial mediation of early diagenesis in the marine water column. *Organic Geochemistry* **26**, 531–544.

Harvey HR, Tuttle JH, Bell JT (1995) Kinetics of phytoplankton decay during simulated sedimentation: changes in biochemical composition and microbial activity under oxic and anoxic conditions. *Geochimica et Cosmochimica Acta* **59**, 3367–3377.

Hayes JM, Freeman KH, Popp BN, Hoham CH (1990) Compound-specific isotopic analyses: a novel tool for reconstruction of ancient biogeochemical processes. *Organic Geochemistry* **16**, 1115–1128.

Hayes JM, Kaplan IR, Wedeking KW (1983) Precambrian organic geochemistry, preservation of the record. In *Earth's Earliest Biosphere: Its Origin and Evolution* (ed. Schopf JW). Princeton University Press, Princeton, NJ, pp. 93–134.

Hayes JM (2001) Fractionation of the isotopes of carbon and hydrogen in biosynthetic processes. *Reviews in Mineralogy and Geochemistry* **43**, 225–278.

Hays LE (2010) *Biogeochemical Proxies for Environmental and Biotic Conditions at the Permian-Triassic Boundary*. Doctoral Dissertation. Massachusetts Institute of Technology Libraries. Available at: http://hdl.handle.net/1721.1/59738.

Hebting Y, Schaeffer P, Behrens A, Adam P, Schmitt G, Schneckenburger P, Bernasconi SM, Albrecht P (2006) Biomarker evidence for a major preservation pathway of sedimentary organic carbon. *Science* **312**, 1627–1631.

Hedges JI, Keil RG (1995) Sedimentary organic matter preservation: an assessment and speculative synthesis. *Marine Chemistry* **49**, 81–115.

Hedges JI, Hu FS, Devol AH, Hartnett HE, Tsamakis E, Keil RG (1999) Sedimentary organic matter preservation: a test for selective degradation under oxic conditions. *American Journal of Science* **299**, 529–555.

Henrichs SM (1992) Early diagenesis of organic matter in marine sediments: progress and perplexity. *Marine Chemistry* **39**, 119–149.

Hieshima GB (1992) *Organic and Isotopic Geochemical Study of the Middle Proterozoic Nonesuch Formation, North American Midcontinent Rift*. Doctoral Dissertation, Indiana University, Indiana. Available from ProQuest Dissertations and Theses Full Text database (UMI No. AAT 9231552). http://proquest.umi.com/pqdweb?did=747640511&Fmt=2&clientId= 79356&RQT=309&VName=PQD.

Hinrichs K-U (2002) Microbial fixation of methane carbon at 2.7 Ga: was an anaerobic mechanism possible? *Geochemistry Geophysics Geosystems* **3**, 1042, 10 pp.

Hoering T (1965) The extractable organic matter in Precambrian rocks and the problem of contamination. *Year Book – Carnegie Institution of Washington* **64**, 215–218.

Hoering T (1967) Criteria for suitable rocks in Precambrian organic geochemistry. *Year Book – Carnegie Institution of Washington* **65**, 365–372.

Höld IM, Schouten S, Jellema J, Sinninghe Damsté JS (1999) Origin of free and bound mid-chain methyl alkanes in oils, bitumens and kerogens of the marine, Infracambrian Huqf Formation (Oman). *Organic Geochemistry* **30**, 1411–1428.

Hollander DJ, Sinninghe Damste JS, Hayes JM, de Leeuw JW, Huc AY (1993) Molecular and bulk isotopic analyses of organic matter in marls of the Mulhouse Basin (Tertiary, Alsace, France). *Organic Geochemistry* **20**, 1253–1263.

Hotinski RM, Kump LR, Arthur MA (2004) The effectiveness of the Paleoproterozoic biological pump: a $\delta^{13}C$ gradient from platform carbonates of the Pethei Group (Great Slave Lake Supergroup, NWT). *Geological Society of America Bulletin* **116**, 539–554.

House CH, Schopf JW, Stetter KO (2003) Carbon isotopic fractionation by Archaeans and other thermophilic prokaryotes. *Organic Geochemistry* **34**, 345–356.

Jahnke RA, Craven DB (1995) Quantifying the role of heterotrophic bacteria in the carbon cycle: a need for respiration rate measurements. *Limnology and Oceanography* **40**, 436–441.

Jiang L, Schofield OME, Falkowski PG (2005) Adaptive evolution of phytoplankton cell size. *The American Naturalist* **166**, 496–505.

Joachimski MM, Ostertag-Henning C, Pancost RD, Strauss H, Freeman KH, Littke R, Sinninghe Damsté JS, Racki G (2001) Water column anoxia, enhanced productivity and concomitant changes in $\delta^{13}C$ and $\delta^{34}S$ across the Frasnian–Famennian boundary (Kowala – Holy Cross Mountains/Poland). *Chemical Geology* **175**, 109–131.

Johnston DT, Wolfe-Simon F, Pearson A, Knoll AH (2009) Anoxygenic photosynthesis modulated Proterozoic oxygen and sustained Earth's middle age. *Proceedings of the National Academy of Sciences of the USA* **106**, 16925–16929.

van Kaam-Peters HME, Schouten S, de Leeuw JW, Sinninghe Damsté JS (1997) A molecular and carbon isotope biogeochemical study of biomarkers and kerogen pyrolysates of the Kimmeridge Clay Facies: palaeoenvironmental implications. *Organic Geochemistry* **27**, 399–422.

Kashiyama Y, Ogawa NO, Kuroda J, Shiro M, Nomoto S, Tada R, Kitazato H, Ohkouchi N (2008a) Diazotrophic cyanobacteria as the major photoautotrophs during mid-Cretaceous oceanic anoxic events: nitrogen and carbon isotopic evidence from sedimentary porphyrin. *Organic Geochemistry* **39**, 532–549.

Kashiyama Y, Ogawa NO, Shiro M, Tada R, Kitazato H, Ohkouchi N (2008b) Reconstruction of the biogeochemistry and ecology of photoautotrophs based on the nitrogen and carbon isotopic compositions of vanadyl porphyrins from Miocene siliceous sediments. *Biogeosciences* **5**, 797–816.

Kelly AE (2009) *Hydrocarbon Biomarkers for Biotic and Environmental Evolution through the Neoproterozoic-Cambrian Transition*. Doctoral Dissertation. Massachusetts Institute of Technology Libraries. Available at: http://hdl.handle.net/1721.1/52763.

Knoll AH, Summons RE, Waldbauer JR, Zumberge JE (2007) The geological succession of primary producers in the oceans. In *Evolution of Primary Producers in the Sea* (eds Falkowski PG, Knoll AH). Elsevier Academic Press, Burlington, MA, pp. 133–163.

Kodner RB, Summons RE, Knoll AH (2009) Phylogenetic investigation of the aliphatic, non-hydrolyzable biopolymer algaenan, with a focus on green algae. *Organic Geochemistry* **40**, 854–862.

Li WKW (1994) Primary production of prochlorophytes, cyanobacteria, and eucaryotic ultraphytoplankton: measurements from flow cytometric sorting. *Limnology and Oceanography* **39**, 169–175.

Logan GA, Hayes JM, Hieshima GB, Summons RE (1995) Terminal Proterozoic reorganization of biogeochemical cycles. *Nature* **376**, 53–56.

Logan GA, Summons RE, Hayes JM (1997) An isotopic biogeochemical study of Neoproterozoic and Early Cambrian sediments from the Centralian Superbasin, Australia. *Geochimica et Cosmochimica Acta* **61**, 5391–5409.

Logan GA, Calver CR, Gorjan P, Summons RE, Hayes JM, Walter MR (1999) Terminal Proterozoic mid-shelf benthic microbial mats in the Centralian Superbasin and their environmental significance. *Geochimica et Cosmochimica Acta* **63**, 1345–1358.

Love GD, Grosjean E, Stalvies C, Fike Da, Grotzinger JP, Bradley AS, Kelly AE, Bhatia M, Meredith W, Snape CE, Bowring SA, Condon DJ, Summons RE (2009) Fossil steroids record the appearance of Demospongiae during the Cryogenian period. *Nature* **457**, 718–721.

Marañón E, Fernández A, Mouriño-Carballido B, Martínez-García S, Teira E, Cermeño P, Chouciño P, Huete-Ortega M, Fernández E, Calvo-Díaz A, Morán XAG, Bode A, Moreno-Ostos E, Varela MM, Patey MD, Achterberg EP (2010) Degree of oligotrophy controls the response of microbial plankton to Saharan dust. *Limnology and Oceanography* **55**, 2339–2352.

Martin JH, Knauer GA, Karl DM, Broenkow WW (1987) VERTEX: carbon cycling in the northeast Pacific. *Deep Sea Research Part A. Oceanographic Research Papers* **34**, 267–285.

McFadden KA, Huang J, Chu X, Jiang G, Kaufman AJ, Zhou C, Yuan X, Xiao S (2008) Pulsed oxidation and biological evolution in the Ediacaran Doushantuo Formation. *Proceedings of the National Academy of Sciences of the USA* **105**, 3197–3202.

Middelburg JJ (1989) A simple rate model for organic matter decomposition in marine sediments. *Geochimica et Cosmochimica Acta* **53**, 1577–1581.

Middelburg J, Vlug T, van der Nat F (1993) Organic matter mineralization in marine systems. *Global and Planetary Change* **8**, 47–58.

Nabbefeld B, Grice K, Twitchett RJ, Summons RE, Hays L, Böttcher ME, Asif M (2010) An integrated biomarker, isotopic and palaeoenvironmental study through the Late Permian event at Lusitaniadalen, Spitsbergen. *Earth and Planetary Science Letters* **291**, 84–96.

Nguyen R, Harvey HR, Zang X, van Heemst JDH, Hetenyi M, Hatcher PG (2003) Preservation of algaenan and proteinaceous material during the oxic decay of *Botryococcus braunii* as revealed by pyrolysis-gas chromatography/mass spectrometry and ^{13}C NMR spectroscopy. *Organic Geochemistry* **34**, 483–497.

Pardue JW, Scalan RS, van Baalen C, Parker PL (1976) Maximum carbon isotope fractionation in photosynthesis by blue-green algae and a green alga. *Geochimica et Cosmochimica Acta* **40**, 309–312.

Popp BN, Laws EA, Bidigare RR, Dore JE, Hanson KL, Wakeham SG (1998) Effect of phytoplankton cell geometry on carbon isotopic fractionation. *Geochimica et Cosmochimica Acta* **62**, 69–77.

Preuß A, Schauder R, Fuchs G (1989) Carbon isotope fractionation by autotrophic bacteria with three different CO_2 fixation pathways. *Zeitschrift für Naturforschung* **44c**, 397–402.

Price GD, Sültemeyer D, Klughammer B, Ludwig M, Badger MR (1998) The functioning of the CO_2 concentrating mechanism in several cyanobacterial strains: a review of general physiological characteristics, genes, proteins, and recent advances. *Canadian Journal of Botany* **76**, 973–1002.

Raven JA (1998) The twelfth Tansley Lecture, small is beautiful: the picophytoplankton. *Functional Ecology* **12**, 503–513.

Richardson TL, Jackson GA (2007) Small phytoplankton and carbon export from the surface ocean. *Science* **315**, 838–840.

Riding R (2006) Cyanobacterial calcification, carbon dioxide concentrating mechanisms, and Proterozoic-Cambrian changes in atmospheric composition. *Geobiology* **4**, 299–316.

Robinson JJ, Cavanaugh CM (1995) Expression of form I and form II Rubisco in chemoautotrophic symbioses: implications for the interpretation of stable carbon isotope values. *Limnology and Oceanography* **40**, 1496–1502.

Roeske CA, O'Leary MH (1985) Carbon isotope effect on carboxylation of ribulose bisphosphate catalyzed by ribulose bisphosphate carboxylase from Rhodospirillum rubrum. *Biochemistry* **24**, 1603–1607.

Rothman DH, Forney DC (2007) Physical model for the decay and preservation of marine organic carbon. *Science* **316**, 1325–1328.

Schidlowski M (1987) Application of stable carbon isotopes to early biochemical evolution on Earth. *Annual Review of Earth and Planetary Sciences* **15**, 47–72.

Schouten S, Klein Breteler W, Blokker P, Schogt N, Rijpstra W, Grice K, Baas M, Sinninghe Damsté JS (1998) Biosynthetic effects on the stable carbon isotopic compositions of algal lipids: implications for deciphering the carbon isotopic biomarker record. *Geochimica et Cosmochimica Acta* **62**, 1397–1406.

Schwab V, Spangenberg JE (2004) Organic geochemistry across the Permian–Triassic transition at the Idrijca Valley, Western Slovenia. *Applied Geochemistry* **19**, 55–72.

Schwab VF, Spangenberg JE (2007) Molecular and isotopic characterization of biomarkers in the Frick Swiss Jura sediments: a palaeoenvironmental reconstruction on the northern Tethys margin. *Organic Geochemistry* **38**, 419–439.

Sinninghe Damsté JS, Kuypers MMM, Pancost RD, Schouten S (2008) The carbon isotopic response of algae (cyano)bacteria, archaea and higher plants to the late Cenomanian perturbation of the global carbon cycle: insights from biomarkers in black shales from the Cape Verde Basin (DSDP Site 367). *Organic Geochemistry* **39**, 1703–1718.

Sirevåg R, Buchanan B, Berry J, Troughton J (1977) Mechanisms of CO_2 fixation in bacterial photosynthesis studied by the carbon isotope fractionation technique. *Archives of Microbiology* **112**, 35–38.

Tchernov D, Lipschultz F (2008) Carbon isotopic composition of *Trichodesmium* spp. colonies off Bermuda: effects of colony mass and season. *Journal of Plankton Research* **30**, 21–31.

Teece M, Fogel M, Dollhopf M, Nealson K (1999) Isotopic fractionation associated with biosynthesis of fatty acids by a marine bacterium under oxic and anoxic conditions. *Organic Geochemistry* **30**, 1571–1579.

Tolosa I, Miquel J-C, Gasser B, Raimbault P, Goyet C, Claustre H (2008) Distribution of lipid biomarkers and carbon isotope fractionation in contrasting trophic environments of the South East Pacific. *Biogeosciences* **5**, 949–968.

Versteegh GJM, Zonneveld KAF (2002) Use of selective degradation to separate preservation from productivity. *Geology* **30**, 615.

Vuorio K, Meili M, Sarvala J (2006) Taxon-specific variation in the stable isotopic signatures ($\delta^{13}C$ and $\delta^{15}N$) of lake phytoplankton. *Freshwater Biology* **51**, 807–822.

Wakeham SG, Lee C, Hedges JI, Hernes PJ, Peterson MJ (1997) Molecular indicators of diagenetic status in marine organic matter. *Geochimica et Cosmochimica Acta* **61**, 5363–5369.

Westrich JT, Berner RA (1984) The role of sedimentary organic matter in bacterial sulfate reduction: the G model tested. *Limnology and Oceanography* **29**, 236–249.

Zonneveld KAF, Versteegh GJM, Kasten S, Eglinton TI, Emeis K-C, Huguet C, Koch BP, de Lange GJ, de Leeuw JW, Middelburg JJ, Mollenhauer G, Prahl FG, Rethemeyer J, Wakeham SG (2010) Selective preservation of organic matter in marine environments; processes and impact on the sedimentary record. *Biogeosciences* **7**, 483–511.

SUPPORTING INFORMATION

Additional Supporting Information may be found in the online version of this article:

Data S1. Derivation and parameterization of models.

Please note: Wiley–Blackwell are not responsible for the content or functionality of any supporting materials supplied by the authors. Any queries (other than missing material) should be directed to the corresponding author for the article.